The Ellipsometry of Chromium–Glass, Nickel–Glass, and Nickel–Chromium–Glass Nanosystems Below and Higher the Néel Temperature

Yevgen Oberemok, Andrii S. Sizhuk, Xiaohong Chen, Zhenjie Zhao, Zhuo Sun, Sergey Savenkov, Vladimir Malyshev, and Oleksandr Prokopenko

Abstract In this work, an investigation of the optical properties for the nanoribbons of nickel on chromium nanofilm and the set of chromium nanofilms is proposed in terms of Mueller ellipsometry. It was observed that if a nickel nanoribbon with a thickness of 250 nm is produced at 250 °C on a chromium film with a thickness of 250 nm, then the experimentally observed state (internal structure) of the nickel nanoribbons is different for the nanosystems, such as nickel nanoribbon-chromium nanofilm and nickel nanoribbon-glass substrate. Despite the opacity of the nickel nanoribbons with the given thicknesses for the used laser light source, the optical properties of the outer surface are thus determined by the interface between the nanoribbon and the type of material of the next layer. For the investigated multilayer nanosystem of the nickel nanoribbons on chromium nanofilm, the global extremum (in the sense of the quadratic dependence indicated above) of the value of the ellipsometric angle is 74.5° for the incident light beam that coincides with the system of chromium nanofilm on glass substrate. At the higher temperature than the Néel temperature for a macroscopic bulk of chromium, the observed abrupt change in the ellipsometric parameters of the nickel nanoribbons on the chromium film is the pretendant to be discussed as the confirmation of the phase transition in the ordering of the internal structure of system with the ferromagnetic–antiferromagnetic interface.

Y. Oberemok · S. Savenkov
Department of Radiophysics, Kyiv National Taras Shevchenko University, Acad. Glushkova Avenue 4-g, Kyiv 03022, Ukraine

A. S. Sizhuk (✉) · V. Malyshev · O. Prokopenko
Institute of High Technologies, Kyiv National Taras Shevchenko University, Acad. Glushkova Avenue 4-g, Kyiv 03022, Ukraine
e-mail: andrii.sizhuk@gmail.com

X. Chen · Z. Zhao · Z. Sun
Physics Department, East China Normal University, Shanghai 200062, China

© The Author(s), under exclusive license to Springer Nature Switzerland AG 2023

O. Fesenko and L. Yatsenko (eds.), *Nanostructured Surfaces, Nanocomposites and Nanomaterials, and Their Applications*, Springer Proceedings in Physics 296,
https://doi.org/10.1007/978-3-031-42704-6_7

1 Introduction

Multicomponent nanofilms, combining ferromagnetic and antiferromagnetic materials, are promising for controlling the specified magnetic and optical properties. For the comparative analysis and construction of the theoretical model, it is important to study the precision antiferromagnetic and ferromagnetic films. In this work, an investigation of the optical properties for the nanoribbons of nickel on chromium nanofilm and the set of chromium nanofilms is proposed. Despite the relatively strong discrete absorption activity of chromium in the optical range, we tested the ellipsometry technique.

Thus, one of the relevant directions of research is the determination of the magnetic properties of nanosamples in a high-frequency electromagnetic field (microwave, infrared, and optical ranges), including the possibility of exciting spin waves by the method of optical pumping.

It is known that a pulsed laser beam in the optical range can excite the propagation of a surface disturbance on a metal surface (for example, plasmon-polaritons, magnons). At the same time, as recent studies show, the spatial configuration (roughness) of the nanoscale can play a determinative role in the efficiency of the interaction between the optical field and the surface perturbation(s) (see, for example, [1–4]). The latter is actual for the systems, in which the generation of spin waves is one of the main effects or mechanisms of scattering and dissipation of electromagnetic energy (see, for example, [5–8]).

In this work, the reflective properties of a set of nickel nanoribbons, deposited on a glass surface and a chromium nanofilm, are described in terms of polarimetry. Experimentally determined ellipsometric parameters make it possible to determine the complex index of refraction of these thin films, in particular Cr–glass substrate, Ni–glass substrate, and Ni–Cr–glass substrate. If quantum transitions in films are not taken into account during light reflection/absorption, then we can say that the complex refractive index depends on the high-frequency conductivity of the multilayer system. At the same time, the considered systems are structures with interface planes (transitions) of the ferromagnet-glass and ferromagnet–antiferromagnet-glass types. It is demonstrated that a 250-nm-thick nickel nanoribbon, sputtered at a temperature of 250 °C on a 250 nm thick chromium film, has different states (internal structures depending on the interface) for such nanosystems as nickel nanoribbon-chromium nanofilm and nickel nanoribbon-glass substrate.

Since our investigation is conducted near the normal conditions, the temperature dependence of the properties of the antiferromagnetic–ferromagnetic interface is also important, since a chromium sample of macroscopic dimensions has its Néel temperature of about 35 °C. At the same time, there is a problem with the application of the concept of temperature for a nanoscale flat system: a relatively rapid change in optical characteristics, when passing through the Néel temperature for chromium, was not observed in the both cases of chromium–glass and nickel–chromium interfaces. Because the concept of temperature can be applied only to macroscopic objects (thermodynamic systems), the explanation of the observed phenomena can be of a

fundamental problem. Strictly speaking, by definition, the measurement procedure of temperature establishes a thermal balance with another macroscopic body. So, in our opinion, there is an important fundamental problem of correctly formulating the state of the nanofilm. Introducing the concept of an equilibrium state, defined by such thermodynamic parameters, as pressure, temperature, and entropy, is not possible for a relatively small, low-dimensional microscopic system, where the predominant interaction is the attraction to the substrate. It is also easy to argue that it is impossible to arbitrarily divide such a low-dimensional (in the space of configurations for the geometry of nanofilms) microscopic system into subsystems without changing the conditions of local dynamic equilibrium with the third macroscopic system (substrate or a thermometer).

Because the optical properties of such nanosystems can be controlled by the temperature of a substrate, there is a potential for applications in programming hardware memory.

1.1 General References

In general, ellipsometry is considered to be an experimental technique that characterizes the composition, roughness, thickness, degree of crystallization, concentration of impurities, electrical conductivity (high-frequency), and other properties of materials (see, for example, [9–13]). Mainly, the data presented here are applicable to the study of the complex refractive index (refractive index) for the obtained chromium films (see previously obtained data and their application in [14, 15]).

The elements of the Mueller matrix M in this work are obtained for four initial Stokes vectors $S_{\text{in}}^{(0)}$, $S_{\text{in}}^{(1)}$, $S_{\text{in}}^{(2)}$, $S_{\text{in}}^{(3)}$, as a solution of the following problem:

$$S_{\text{out}}^{(k)} = M\, S_{\text{in}}^{(k)}, \tag{1}$$

where $S_{\text{in}}^{(k)} = \left(S_{in0}^{(k)}, S_{in1}^{(k)}, S_{in2}^{(k)}, S_{in3}^{(k)}\right)^T$ are the initial Stokes vectors; $M = \left(M_{ij}\right)$, with $(i, j) = (0 \ldots 3, 0 \ldots 3)$, is the Mueller matrix. Note, in the nonstandard notation of the text below, the indexes i, j for the elements of the Mueller matrix run over digits $(1 \ldots 4, 1 \ldots 4)$.

The initial Stoke vectors $S_{\text{in}}^{(k)}$ are prepared in the following way. After passing the linear polarizer (denoted by LP in Fig. 1, see below in the text), the initial Stokes vector becomes defined by the following set of numbers (in the case of normalized calculus):

$$S^{II} = (1, -1, 0, 0)^T. \tag{2}$$

Then, passing through the phase plate (denoted PP) in the polarization generator GP (see the scheme in Fig. 1) the state of the light beam becomes defined as

$$S_{\text{in}} = \begin{pmatrix} 1 \\ \cos^2(2\alpha) + \cos(\Delta)\sin^2(2\alpha) \\ -\cos(2\alpha)\sin(2\alpha)(\cos(\Delta) - 1) \\ \sin(2\alpha)\sin(\Delta) \end{pmatrix}. \tag{3}$$

The sequence of angles for the relative orientation α of the phase plate PP at the fixed phase shift Δ in the polarization generator PG (see Fig. 1) are set to be:

$$\{-52^\circ, -14^\circ, 14^\circ, 51^\circ\}. \tag{4}$$

The corresponding initial Stokes vectors therefore are

$$\begin{aligned} S_{\text{in}}^{(0)} &= (1, 0.768, -0.422, -0.482)^T; \\ S_{\text{in}}^{(1)} &= (1, 0.768, 0.422, 0.482)^T; \\ S_{\text{in}}^{(2)} &= (1, 0.056, 0.230, -0.972)^T; \\ S_{\text{in}}^{(3)} &= (1, 0.056, -0.230, 0.972)^T. \end{aligned} \tag{5}$$

As we noted above, in addition to such surface properties as roughness and crystalline structure, the polarimetry can help to determine the high-frequency electrical resistance (complex impedance) if the quantum nature of absorption (or refraction) is not taken into account (see, for example, [9–17]). In particular, nanoribbons, deposited on chrome surfaces, have many optical properties, which are determined by relatively very optically active chromium. This is also confirmed by experimental data that will be discussed below. To cause elliptic polarization to a linear polarized beam is one of the known important features of metal surfaces. And, the processes of reflection can be nonlinear in intensity, that restricts the use of the essentially linear theory for the Fresnel equations. Nevertheless, the method of the Mueller matrix allows to analyze the contributions to the linear and circular polarizations as the constituents to the state of the elliptically polarized scattered light beam. The presented below ellipsometric angles Ψ and Δ determine the complex refractive index of chromium and nickel thin films (see previously obtained data and their application in [16–18]). The complex refractive index determines the complex dielectric constant. In turn, the imaginary part of the complex dielectric constant is determined by the conductivity of the light-reflecting material. A detailed study of the frequency dependence of the dielectric permittivity makes it possible to formulate a model of the internal structure of the nanosystem (see, for example, [19]). Here, we propose to focus attention on the properties of the system at a given frequency of the optical beam to determine the effect of the antiferromagnet–ferromagnet interface on the optical (impedance) characteristics of the nanosurface.

1.2 The Method of Investigation

The Mueller matrix elements for a set of chromium nanofilms at room temperature are determined by the ellipsometry of the incident and reflected beam (see Fig. 1) for the given four initial polarization states, S_{in}. For a comparison, chromium nanofilms with an average thickness of 132, 151, and 183 nm, obtained by thermal sputtering on a glass substrate, are scanned. The normalized elements of the Mueller matrix as the function of the angle of incidence are shown in the corresponding graphs. The used light source is a He–Ne laser with the wavelength of 633 nm and the power of approximately 15 mW.

The accuracy of the experimental measurements is estimated to be within 2.6%.

There is the schematic illustration of a Muller polarimeter in Fig. 1. The Muller polarimeter consists of a light source S, a polarization generator PG, a phase plate PP, a linear polarizer P, and a photodetector PD.

The sketches of the discovered here samples with the corresponding scanning points are shown in Fig. 2.

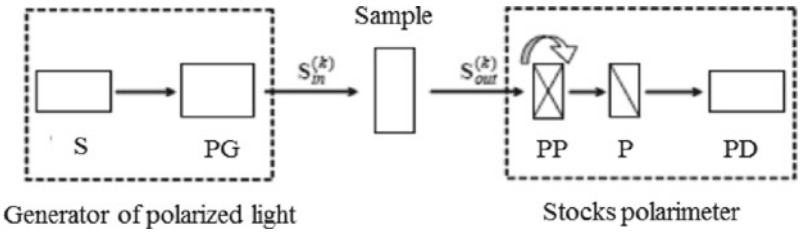

Fig. 1 Schematic illustration of a Muller polarimeter with a light source S, a polarization generator PG, a phase plate PP, a linear polarizer P, and a photodetector PD

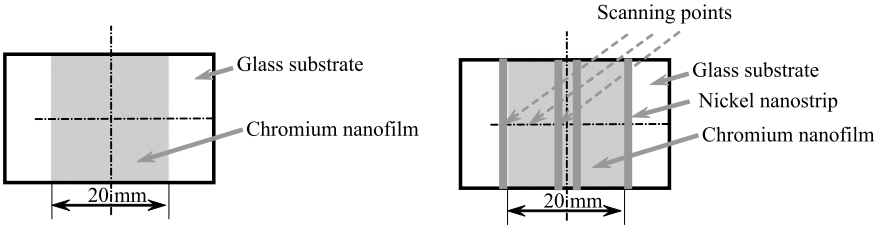

Fig. 2 Locations of the He–Ne laser beam scattering at the topographical sample with the deposited nickel nanostrips

2 The Results of the Experimental Observations and Calculations

The normalized elements M_{12} and M_{43} of the Mueller matrix as the function of the angle of incidence on the chromium nanofilm (for an estimated film thickness of 151 nm) are presented in Fig. 3.

The normalized M_{21} and M_{31} elements of the Mueller matrix as the function of the angle of incidence at the chromium nanofilm (corresponding to an estimated thickness of 132 nm) are shown in Fig. 4.

The corresponding M_{21} and M_{31} function curves for the 151 and 183 nm samples are indistinguishable at this resolution and repeat the dependence contour for the 132 nm thickness.

The normalized elements M_{24} and M_{34} are depicted in Fig. 5.

At the given resolution, the dependences on the angle of incidence are identical for the given set of the samples of different thicknesses.

The normalized elements M_{33} and M_{44} of the Mueller matrix for the thicknesses of 132, 151, and 183 nm are shown in Fig. 6.

The curves for the different thicknesses are indiscernible.

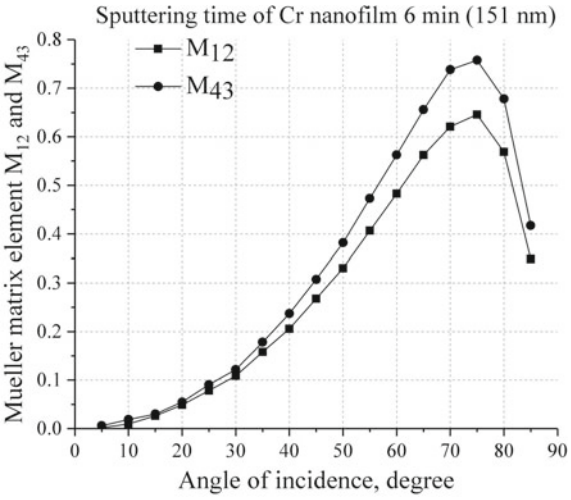

Fig. 3 Normalized elements M12 and M43 of the Mueller matrix as the function of the angle of incidence at the chromium nanofilm. The curves for the samples with the thickness of 132 and 183 nm are visually identical at this resolution and follow the 151 nm curve presented. The data were checked for the same samples through one year, see [20]

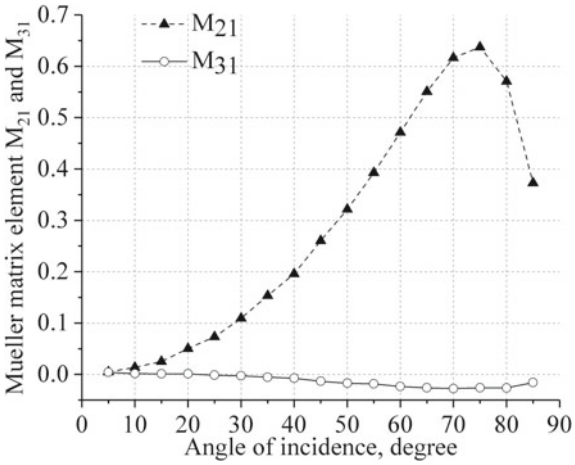

Fig. 4 Normalized elements of the Mueller matrix M_{21} and M_{31} as the functions of the angle of incidence on the chromium nanofilm (corresponding to an estimated thickness of 132 nm). The data were checked for the same samples through one year, see [20]

Fig. 5 Normalized elements M_24 and M_34. The data were checked for the same samples through one year, see [20]

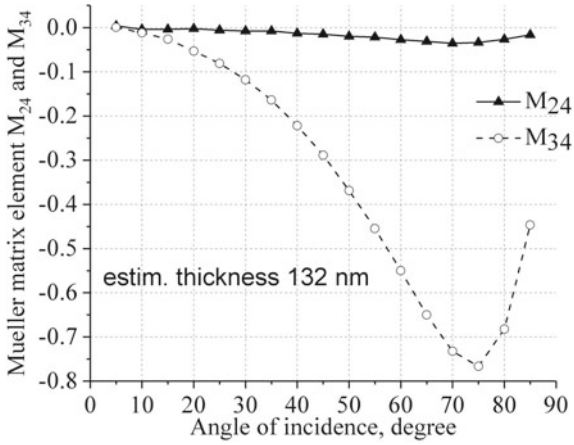

2.1 *The Investigation of the Sample with the Deposited on the Chromium Film Nanoribbons of Nickel at Temperatures Below the Néel point for a Bulk Chromium*

The results of the polarimetry analysis for the metal thin films in the mirror geometry of the experimental setup Fig. 1 are shown in Figs. 7 and 8.

Here, the samples of nickel–chromium nanofilms on a glass substrate with a length of 20 mm, a width of 2 mm, and a thickness of approximately 250 nm were studied at room temperature (below 25 °C).

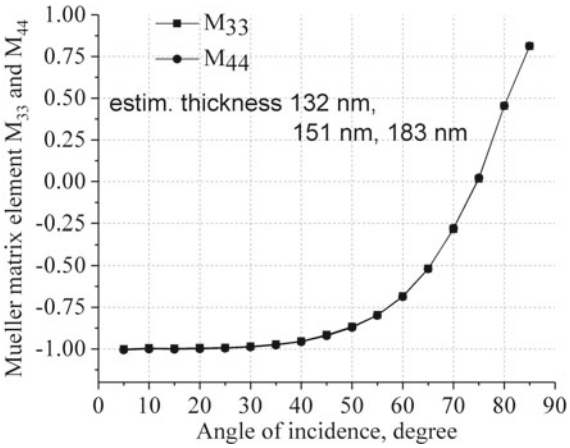

Fig. 6 Normalized elements M_{33} and M_{44}. The data are taken from [20]

As it can be seen from the graphs in Fig. 7, the angle of incidence 74.5° ± 0.25° corresponds to the location of the global extremum of the dependencies for the three types of the nanofilms.

In Figs. 7 and 8, the polarization characteristics (dichroic angles Ψ and phase Δ) for different thicknesses of chromium films coincide within the specified accuracy

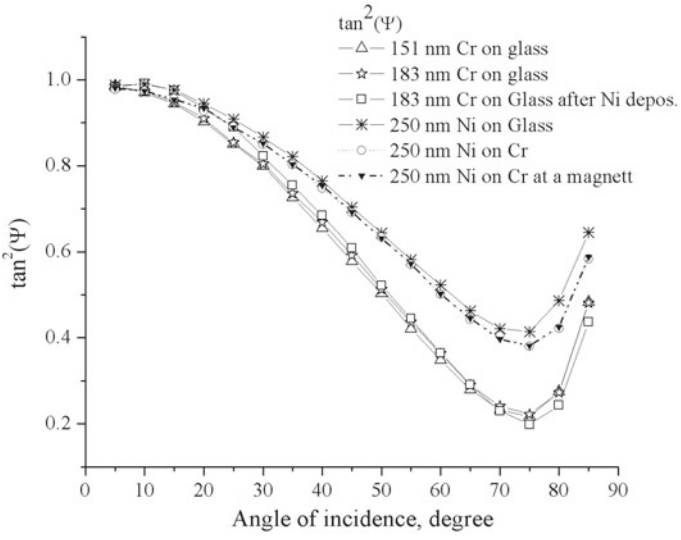

Fig. 7 Squared tangent of the ellipsometric angle Ψ as the function of incidence angle. The data were obtained from the Mueller matrices, experimentally measured for chromium nanofilms on glass, nickel on glass, and nickel on chromium nanofilm on glass. The data are from the work of authors [21]

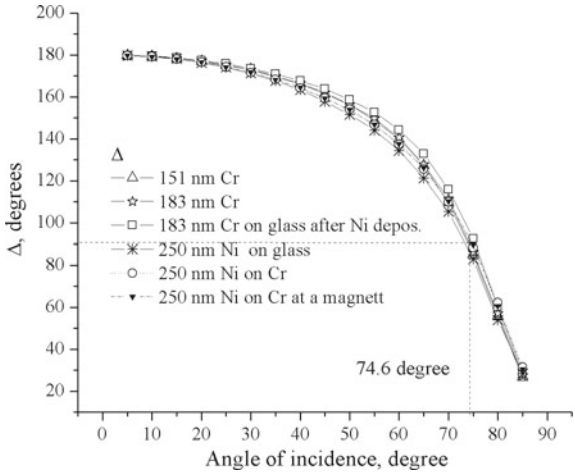

Fig. 8 Ellipsometric angle Δ as the function of incidence angle. The data were obtained from the Mueller matrices experimentally measured for chromium nanofilms on glass, nickel on glass, and nickel on chromium nanofilm on glass. The data are from the work of authors [21]

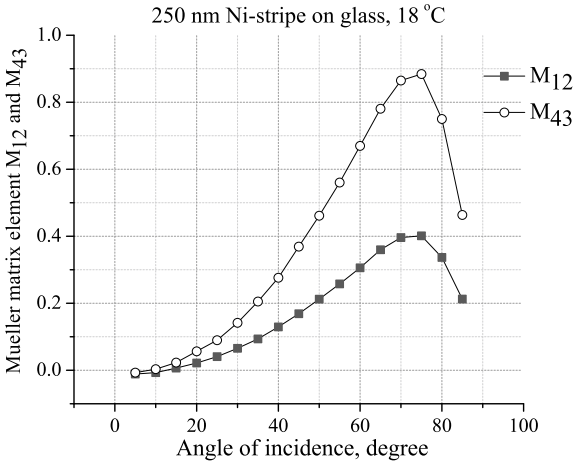

Fig. 9 Normalized (to the M11 element) element M_{12} and M_{43} of the Mueller matrix as the function of the angle of incidence at the nickel nanoribbon. The the nickel nanoribbon was thermally sputtered onto a glass plate (glass temperature during sputtering was approximately 250 °C). The thickness of the nanoribbon is approximately 250 nm

(2.6%). When reflected, the dichroic properties of the directly sputtered onto glass nickel nanoribbons differ significantly from those sputtered onto the chromium film on the glass. The difference in the phase parameters, Δ, of the studied samples is also noticeable within the angle of incidence of 30°−75°. But this difference is less pronounced compared to dichroic characteristics.

To compare the behavior of the Mueller matrix elements, characterizing the nickel, chromium, and glass substrate, the corresponding incidence angle functions of M_{12} (and M_{21}, which has a similar dependence), M_{14}, M_{43} are presented below. The matrix elements are relatively sensitive to the type of a substrate surface.

Figure 9 shows the normalized (to M_{11}) elements M_{12} and M_{43} as the function of incidence angle at a nickel nanoribbon. The nickel nanoribbon was thermally sputtered onto a glass plate (glass temperature during sputtering was approximately 250 °C). The thickness of the nanoribbon is approximately 250 nm.

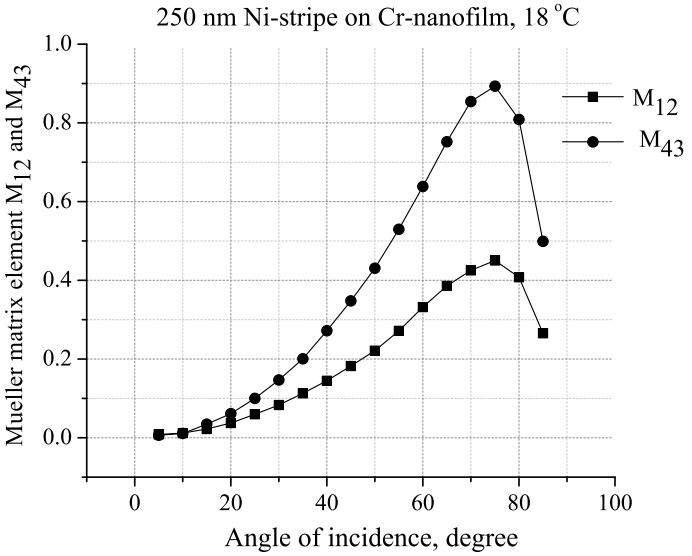

Fig. 10 Normalized element M_{12} and M_{43} of the Mueller matrix as the function of the angle of incidence at the nickel nanoribbon. The nickel layer was thermally sputtered onto chromium nanofilm (with its thickness within 250 nm) on glass at the temperature of 250 °C. The thickness of the nanoribbon is approximately 250 nm

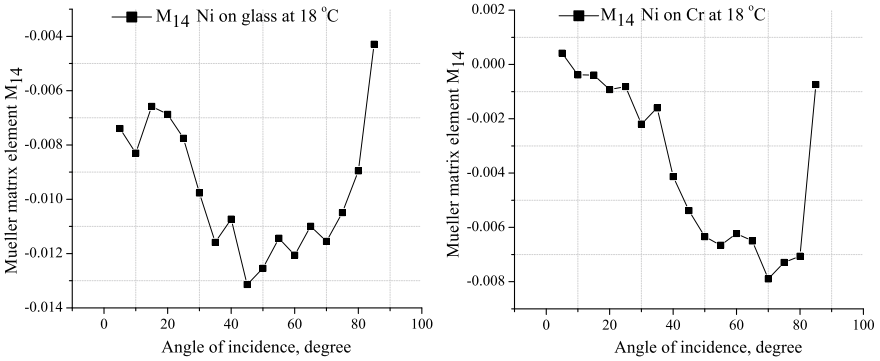

Fig. 11 Normalized element M_{14} (or/and M_{41}) of the Mueller matrix as the function of the angle of incidence at the nickel nanoribbon. The nickel layer was thermally sputtered onto glass or chromium nanofilm (with its thickness within 250 nm) on glass at the temperature of 250 °C. The thickness of the nanoribbon is approximately 250 nm

The graphs in 10 depict the dependence of the normalized element M_{12} and M_{43} of the Mueller matrix from the angle of incidence at the nickel nanoribbon. Here, the nickel layer was thermally deposited onto glass or chromium nanofilm (with a thickness within 250 nm) on glass at the temperature 250 °C. The thickness of the nickel strips is approximately 250 nm. Other Mueller matrix elements for the nanosystem of chrome film-glass substrate are presented by the authors in [20].

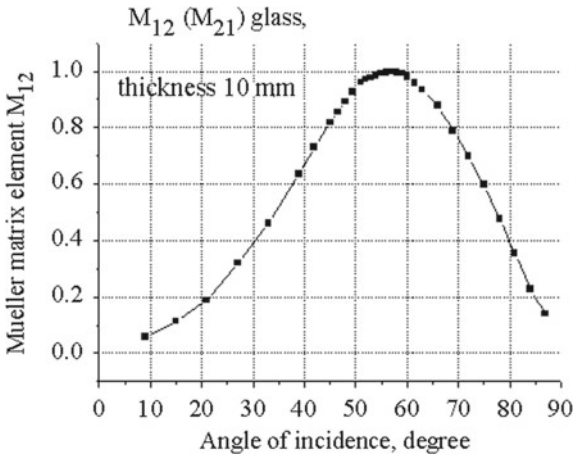

Fig. 12 Normalized element M_{12} (or/and M_{21}) of the Mueller matrix as the function of the incidence angle of a light beam at a glass plate with the thickness of 10 mm. The data are taken from the recent authors' work [21]

In Fig. 11, the normalized (to M_{11}) element M_{14} as the function of incidence angle at a nickel nanoribbon is shown.

The normalized element M_{12} (or/and M_{21}) of the Mueller matrix as the function of the incidence angle of a light beam at a glass plate with the thickness of 10 mm is shown in Fig. 12.

We experimentally investigated that the behavior (form of dependence) of these nanosurfaces of chromium and nickel chemical elements is qualitatively similar. Global extremes are in the range of 73°−75°. Global extrema for the studied materials, mainly for Cr and Ni, are relatively close to the samples with an annealed Au surface (see [21]). This allows us to think about the rather high smoothness of the specified surfaces.

At the same time, the change in the polarization state of the light beam after reflection is more pronounced at the nanosurfaces of ferro(antiferro)magnetic materials. Under certain assumptions, neglecting, for example, the scattering from surface irregularities, the angle of incidence at 74.5° corresponds to Brewster's angle.

The discussed here data are obtained from the experimentation on a sample in air. Thus, the presence of water molecules on the surface of typical chromium or nickel samples causes certain changes in the background reflectance. Some analysis of changes in the refractive index in the presence of a nanolayer of water, depending on temperature regimes, type of substrate, etc., can be found, for example, in [22–25].

2.2 The Investigation of the Sample with the Deposited on the Chromium Film Nanoribbons of Nickel at Temperatures Higher the Néel Point for a Bulk Chromium

Here, we describe the observation of a phase transition of the internal structural ordering for the ferromagnetic nickel nanostrip on an antiferromagnetic surface of chromium at a temperature above the Néel temperature for "macroscopic" chromium.

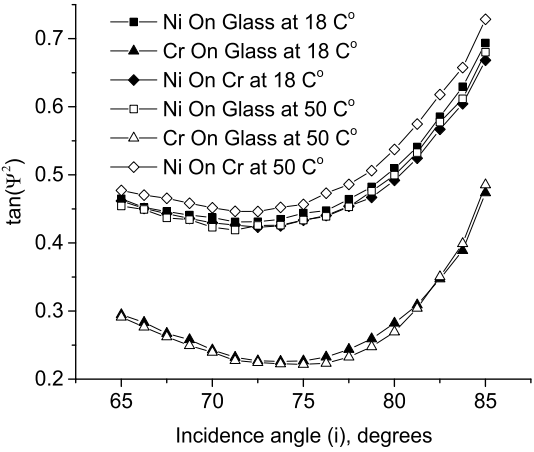

Fig. 13 Angular dependences of ellipsometric parameter Ψ at temperatures of 18 °C and 50 °C

Nickel nanostrips with a thickness of 250 nm and a width of about 2 mm on glass (the side strips in Fig. 2) and on a chrome film on glass (the central two strips in Fig. 2) were produced by the method of thermal sputtering using the VUP-5M system.

At temperatures around 20−40 °C, significant changes in the values of ellipsometric parameters were not observed for this topographic sample, even with the passage of a relatively significant period of time, which is about one year. But, at a temperature of about 50 °C, the behavior of the nickel nanoribbon on chromium changes significantly compared to room temperatures (see Figs. 13 and 14). At the same time, changes in the values of ellipsometric parameters for chromium on glass and nickel on glass are detectable but relatively small.

Moreover, unlike chromium–glass and nickel–glass systems, the nickel–chromium–glass system increases the value of the dichroic angle Ψ with increasing temperature at the extremum. Hence, at the significantly higher temperature than the Néel temperature for a macroscopic bulk of chromium, the observed abrupt change in the ellipsometric parameters is the pretendant to be discussed as the confirmation of the phase transition in the ordering of the internal structure of the ferromagnetic nickel nanostrip on the antiferromagnetic surface of chromium.

Figure 15 shows the normalized (to M_{11}) element M_{12} (or/and M_{21}) and M_{43} as the function of incidence angle at a chromium nanofilm thermally sputtered onto a glass plate. The thickness of the nanofilm is approximately 250 nm.

Figure 16 shows the normalized (to M_{11}) element M_{12} (or/and M_{21}) and M_{43} as the function of incidence angle at a nickel nanoribbon thermally sputtered onto a glass plate and chromium film on glass (glass temperature during sputtering was approximately 250 °C). The thickness of the nanoribbon is approximately 250 nm. The temperature of the glass substrate during the scanning was 50 °C.

Figure 17 shows the normalized (to M_{11}) element M_{14} as the function of incidence angle at a nickel nanoribbon thermally sputtered onto a glass plate and chromium film on glass (glass temperature during sputtering was approximately 250 °C). The thickness of the nanoribbon is approximately 250 nm. The temperature of the glass substrate during the scanning was 50 °C.

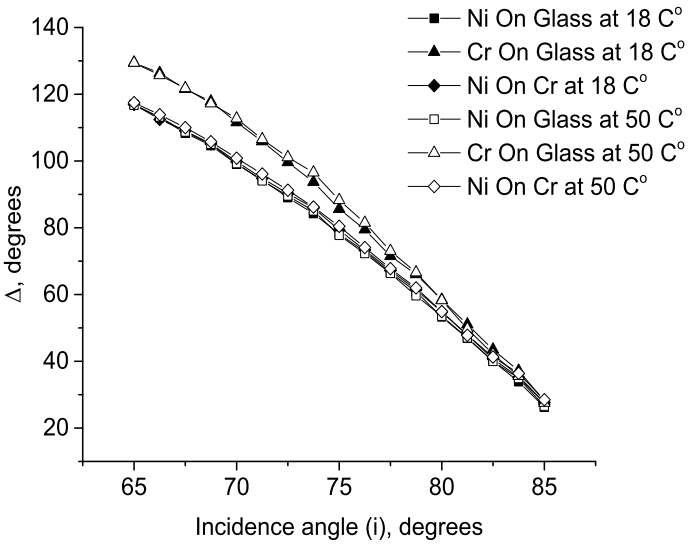

Fig. 14 Angular dependences of ellipsometric parameter Δ at temperatures of 18 °C and 50 °C

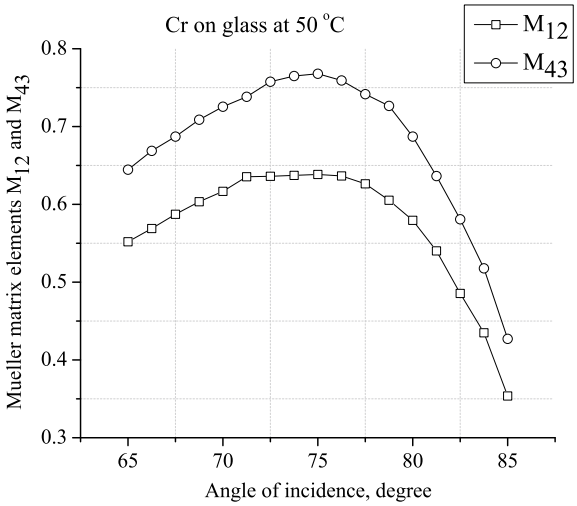

Fig. 15 Normalized (to the M11 element) element M_{12} (or/and M_{21}) of the Mueller matrix as the function of the angle of incidence at a chromium nanofilm thermally sputtered onto a glass plate. The thickness of the nanofilm is approximately 250 nm. The temperature of the glass substrate during the scanning was 50 °C

It is interesting to note that, in comparison with the other elements of the matrix, such term as M_{41}, for the multilayer systems of Ni on Cr and Ni on glass at 50 °C, shows significant difference in values (see the graphs in Fig. 18). The change in sign of the quantity can be referred to the existence of certain critical point. In case of the

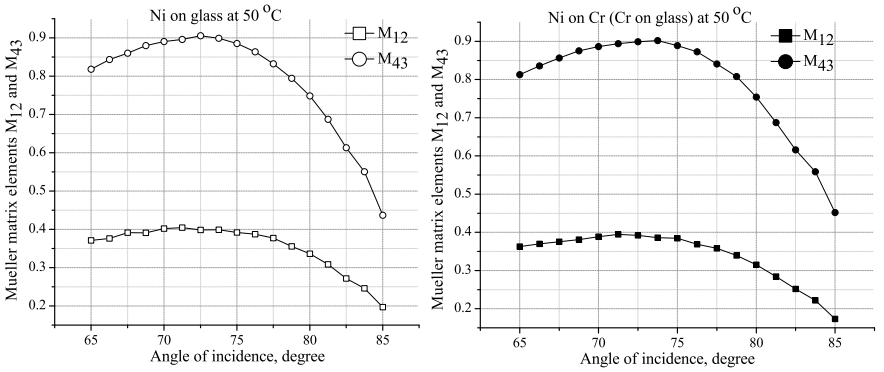

Fig. 16 Normalized (to the M11 element) element M_{12} (or/and M_{21}) of the Mueller matrix as the function of the angle of incidence at the nickel nanoribbon thermally sputtered onto a glass plate and chromium film on glass (glass temperature during sputtering was approximately 250 °C). The thickness of the nanoribbon is approximately 250 nm. The temperature of the glass substrate during the scanning was 50 °C

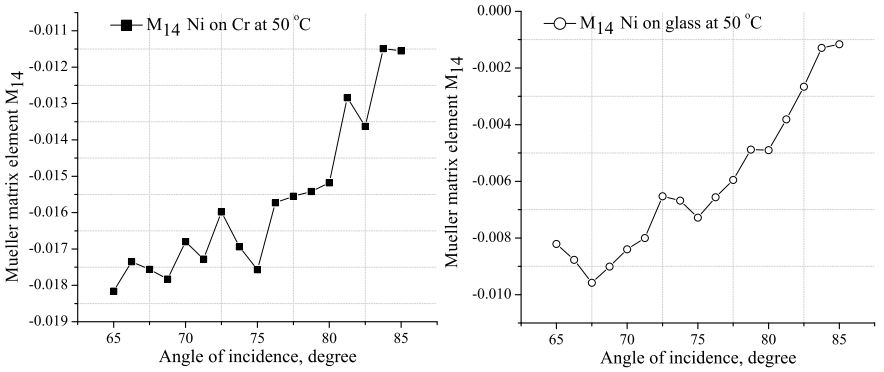

Fig. 17 Normalized (to the M11 element) element M_{14} of the Mueller matrix as the function of the angle of incidence at the nickel nanoribbon thermally sputtered onto a glass plate and chromium film on glass (glass temperature during sputtering was approximately 250 °C). The thickness of the nanoribbon is approximately 250 nm. The temperature of the glass substrate during the scanning was 50 °C

ferromagnetic–antiferromagnetic interface, the latter is supposed to be related to a phase transition in the intrinsic order of the films.

By the multiplication rules for matrix (1), in accordance with the definition, the element M_{41} contributes to the $S_{out3}^{(k)}$ element of the final Stokes vector through the additive term $M_{41} S_{in0}^{(k)}$. The term $S_{out3}^{(k)}$ describes, by the definition of the Stokes vector, the order of the circular polarization of the scattered beam, while the element $S_{in0}^{(k)}$ of the initial Stokes vector is related to the initial intensity of the incoming light beam. Thus, depending on the temperature of the substrate, the contribution to the circular polarization of the scattered beam is

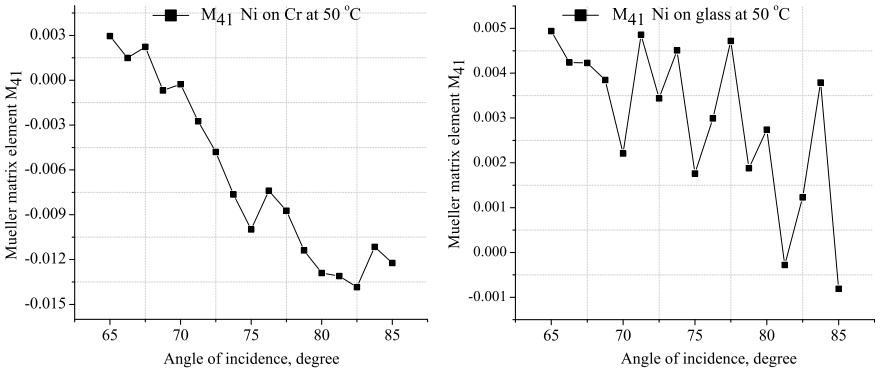

Fig. 18 Normalized (to the M11 element) element M_{41} of the Mueller matrix as the function of the angle of incidence at the nickel nanoribbon thermally sputtered onto a glass plate and chromium film on glass (glass temperature during sputtering was approximately 250 °C). The thickness of the nanoribbon is approximately 250 nm. The temperature of the glass substrate during the scanning was 50 °C

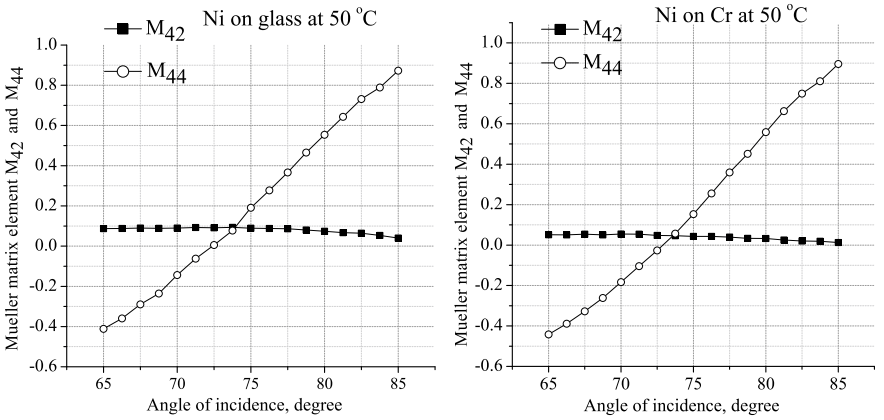

Fig. 19 Normalized (to the M_{11} element) elements M_{42} and M_{44} as the function of the angle of incidence at the nickel nanoribbon on the chromium nanofilm and on the glass substrate at 50 °C. The nanoribbons were thermally sputtered onto a glass plate (glass temperature during sputtering was approximately 250 °C). The thickness of the nanoribbon is approximately 250 nm

$$S_{\text{out3}} = M_{41}S_{\text{in0}} + M_{42}S_{\text{in1}} + M_{43}S_{\text{in2}} + M_{44}S_{\text{in3}}. \tag{6}$$

The above term S_{out3} can therefore be found using the corresponding Mueller matrix elements M_{41}, M_{42}, M_{43}, M_{44} and the initial polarization state vector (Stokes vector) S_{in}. By analogy, it can be found the rest of the final Stokes vector S_{out}. The rest of the needed for this elements M_{42} and M_{44} for the nickel nanoribbon on the chromium nanofilm on glass substrate at 50 °C are provided in Fig. 19.

The influence of the crystalline substructures of the nanolayers and the substrate on the formation of structured nanofilms of nickel and chromium also takes place (see [8]), as was observed for silicon substrates in [13, 14]. The latter strongly depends on the temperature of the substrate during the deposition process. The oxidation process (see [6] and the refractive index tables in [15]) also changes the reflective and absorptive properties of the surface.

3 Conclusions

In this research, the light reflection properties of the collection of nanoribbons, sputtered onto a glass plate, are described in terms of polarimetry. Experimentally obtained ellipsometric parameters allow to determine the complex index of refraction for Ni–Cr–glass, Cr–glass, and Ni–glass nanostructures.

The global maximum (minimum) of elements M_{12}, M_{43}, M_{21}, M_{31}, M_{24}, M_{34} for the samples of chromium with the thicknesses of 132, 151, and 183 nm was observed at approximately 74.5°. If the residual scattering and absorption of light by the surface are neglected for this angle of incidence, then the Brewster angle for the system under investigation is assumed to be 74.5 ° with the given measurement accuracy.

No significant dependence on the film thickness of chromium was observed for such matrix elements as M_{12}, M_{43}, M_{21}, M_{31}, M_{24}, M_{34}, M_{33}, and M_{44}.

If a nickel nanoribbon with a thickness of 250 nm is produced at 250 °C on a chromium film with a thickness of 250 nm, then the experimentally observed state (internal structure) of the nickel nanoribbons is different for the nanosystems, such as nickel nanoribbon-chromium nanofilm and nickel nanoribbon-glass substrate. Despite the opacity of the nickel nanoribbons with the given thicknesses for the used laser light source, the optical properties of the outer surface are thus determined by the interface between the nanoribbon and the type of material of the next layer.

At the higher temperature than the Néel temperature for a macroscopic bulk of chromium, the observed abrupt change in the ellipsometric parameters of the nickel nanoribbons on the chromium film is the pretendant to be discussed as the confirmation of the phase transition in the ordering of the internal structure of system with the ferromagnetic–antiferromagnetic interface.

For the investigated multilayer nanosystems the nickel nanoribbons, the global extremum (in the sense of the quadratic dependence indicated above) of the value of the ellipsometric angle is 74.5° for the incident light beam.

Acknowledgements This work was supported in part by the grant No. 22BF07-03 from the Ministry of Education and Science of Ukraine.

References

1. E. L. Gurevich, S. V. Gurevich, Laser induced periodic surface structures induced by surface plasmons coupled via roughness. Appl. Surf. Sci. **302**, 118–123 (2014). https://doi.org/10.1016/j.apsusc.2013.10.141
2. M. Ardron, N. Weston, D. Hand, A practical technique for the generation of highly uniform LIPSS. Appl. Surf. Sci. **313**, 123–131 (2014). https://doi.org/10.1016/j.apsusc.2014.05.154
3. M. Huang, F. Zhao, N. Xu. Y. Cheng, Origin of laser-induced near-subwavelength ripples: interference between surface plasmons and incident laser. ACS Nano **3**(12), 4062–4070 (2009)
4. K. Zhou, X. Jia, T. Jia, K. Cheng, K. Cao, S. Zhang, D. Feng, Z. Sun, The influences of surface plasmons and thermal effects on femtosecond laser-induced subwavelength periodic ripples on Au film by pump-probe imaging. J. Appl. Phys. **121**, 104301 (2017). https://doi.org/10.1063/1.4978375
5. A. Kamimaki, S. Iihama, Y. Sasaki, Y. Ando, Micro-focused pulse laser-induced propagating spin waves in permalloy films with different thicknesses. IEEE Trans. Magn. (99), 1–1 (2017)
6. T. Ohkochi, *Gigantic Spin Waves Induced by Ultrashort Laser Pulses* (Research Frontiers, Physical Science, 2017), pp. 44–45
7. S. Kolodny, D. Yudin, I. Iorsh, Resonant spin wave excitation in magnetoplasmonic bilayers using short laser pulses. Nanoscale **11**, 2003–2007 (2019)
8. A.A. Awad, S. Muralidhar, A. Aleman, R. Khymyn, M. Dvornik, D. Lu, D. Hanstorp, J. Akerman, *Stimulated k-vector Selective Magnon Emission in NiFe Films Using Femtosecond Laser Pulse Trains*. arXiv:1908.03388v1 [cond-mat.mes-hall] (2019)
9. R.M.A. Azzam, M. Elshazly-Zaghloul, N.M. Bashara, Combined reflection and transmission thin-film ellipsometry: a unified linear analysis. Appl. Optics **14**(7), 1652–1663 (1975). https://doi.org/10.1364/AO.14.001652
10. I. Ohlidal, E. Schmidt, M. Libezny, Complete unambiguous optical characterization of double layers consisting of two strongly absorbing thin films by combined reflection and transmission ellipsometry. Appl. Optics **29**(4), 593–598 (1990). https://doi.org/10.1364/AO.29.000593
11. G. Bader, P.V. Ashrit, V.-V. Truong, Transmission and reflection ellipsometry of thin films and multilayer systems. Appl. Optics **37**(7), 1146–1151 (1998). https://doi.org/10.1364/AO.37.001146
12. J. Toudert, Spectroscopic ellipsometry for active nano- and meta-materials. Nanotechnol. Rev. **3**(3), 223–245 (2014). https://doi.org/10.1515/ntrev-2013-0043
13. P.B. Johnson, R.W. Christy, Optical constants of transition metals: Ti, V, Cr, Mn, Fe, Co, Ni, and Pd. Phys. Rev. B **9**, 5056 (1973). https://doi.org/10.1103/PhysRevB.9.5056
14. D.A. Rakić, A.B. Djurišić, J.M. Elazar, M.L. Majewski, Optical properties of metallic films for vertical-cavity optoelectronic devices. J. Optical Soc. Am. **37**, 5271–5283 (1998). https://doi.org/10.1364/AO.37.005271
15. H.G. Tompkins, J. Baker, D. Convey, Effect of process parameters on the optical constants of thin metal films. Surface and Interface Analysis **29**, 227–231 (2000)
16. J. Wang, J. Dong, Y. Cheng, Z. Xie, Y. Chen, Visible to near-infrared perfect absorption from alternate silica and chromium layers deposited by magnetron sputtering. Optics Lett. **46**, 4582–485 (2021)
17. T. Grigor'eva, T. Khasanov, Optical constants of Ni nanofilms. Optics Spectrosc. **112**, 796–800 (2012)
18. K.-Y. Chou, C.-L. Wu, C.-C. Shen, J.-K. Sheu, C.-K. Sun, Terahertz photoacoustic generation using ultrathin nickel nanofilms. J. Phys. Chem. C **125**(5), 3134–3142 (2021). https://doi.org/10.1021/acs.jpcc.0c09303
19. P.Y. Yu, M. Cardona, *Fundamentals of Semiconductors: Physics and Materials Properties* (Springer, Berlin, 2001), p. 261. ISBN 978-3-540-25470-6
20. Y. Oberemok, S. Savenkov, X. Chen, Z. Zhao, Z. Sun, A. Sizhuk, O. Prokopenko, Mueller matrix for chromium nanofilms on a glass substrate, in *2021 IEEE 11th International Conference Nanomaterials: Applications Properties (NAP)* (2021), pp. 1–5. https://doi.org/10.1109/NAP51885.2021.9568513

21. Y. Oberemok, S. Savenkov, X. Chen, Z. Zhao, Z. Sun, A. Sizhuk, O. Prokopenko, V. Malyshev, K. Yakimov, T. Rodionova, Polarimetry For Nickel-Chromium two-layer nanofilms and Nickel nanostripe on a glass substrate, in *2022 IEEE 41st International Conference on Electronics and Nanotechnology (ELNANO)* (2022), pp. 224–227. https://doi.org/10.1109/ELNANO54667.2022.9927127
22. F. McCrackin, E. Passaglia, R. Stromberg, H. Steinberg, Measurement of the thickness and refractive index of very thin films and the optical properties of surfaces by ellipsometry. J. Res. Natl. Bureau Stand. A. Phys. Chem. **67A**(4), 363–377 (1963)
23. M. Aouadi, D.M. Mihut, M.L. Kuruppu, S.R. Kirkpatrick, S.L. Rohde, Spectroscopic ellipsometry measurements of chromium nitride coatings. J. Vac. Sci. Technol. A **19**(6), 2800–2804 (2001)
24. J.A. Solovjov, V.A. Pilipenko, Effect of rapid thermal treatment temperature on electrophysical properties of Nickel films on Silicon. Doklady BGUIR **18**(1), 81–88 (2020)
25. T. Ivanova, K.A. Gesheva, A. Szekeres, O. Trofimov, Surface characterization of Chromium Oxide thin films in dependence on CVD growth process parameter. ECS Trans. **2**, 229–236 (2007)